UC Davis

UC Davis Previously Published Works

Title

ErbB2 regulates autophagic flux to modulate the proteostasis of APP-CTFs in Alzheimer's disease

Permalink

https://escholarship.org/uc/item/1zn1t4v2

Journal

Proceedings of the National Academy of Sciences of the United States of America, 114(15)

ISSN

0027-8424

Authors

Wang, Bo-Jeng
Her, Guor Mour
Hu, Ming-Kuan
et al.

Publication Date

2017-04-11

DOI

10.1073/pnas.1618804114

Peer reviewed

eScholarship.org Powered by the California Digital Library
University of California

ErbB2 regulates autophagic flux to modulate the proteostasis of APP-CTFs in Alzheimer's disease

Bo-Jeng Wang[a], Guor Mour Her[b,c], Ming-Kuan Hu[d], Yun-Wen Chen[a], Ying-Tsen Tung[a], Pei-Yi Wu[a], Wen-Ming Hsu[e], Hsinyu Lee[f], Lee-Way Jin[g], Sheng-Ping L. Hwang[a], Rita P.-Y. Chen[h], Chang-Jen Huang[h], and Yung-Feng Liao[a,f,1]

[a]Institute of Cellular and Organismic Biology, Academia Sinica, Taipei 11529, Taiwan; [b]Institute of Bioscience and Biotechnology, National Taiwan Ocean University, Keelung 20224, Taiwan; [c]Center of Excellence for Marine Bioenvironment and Biotechnology, National Taiwan Ocean University, Keelung 20224, Taiwan; [d]School of Pharmacy, National Defense Medical Center, Taipei 114, Taiwan; [e]Department of Surgery, National Taiwan University Hospital and National Taiwan University College of Medicine, Taipei 10002, Taiwan; [f]Department of Life Science, National Taiwan University, Taipei 10617, Taiwan; [g]Department of Pathology and Laboratory Medicine, Alzheimer's Disease Center, University of California Davis Medical Center, Sacramento, CA 95817; and [h]Institute of Biological Chemistry, Academia Sinica, Taipei 11529, Taiwan

Edited by Solomon H. Snyder, Johns Hopkins University School of Medicine, Baltimore, MD, and approved March 7, 2017 (received for review November 14, 2016)

Proteolytic processing of amyloid precursor protein (APP) C-terminal fragments (CTFs) by γ-secretase underlies the pathogenesis of Alzheimer's disease (AD). An RNA interference screen using APP-CTF [99-residue CTF (C99)]- and Notch-specific γ-secretase interaction assays identified a unique ErbB2-centered signaling network that was predicted to preferentially govern the proteostasis of APP-C99. Consistently, significantly elevated levels of ErbB2 were confirmed in the hippocampus of human AD brains. We then found that ErbB2 effectively suppressed autophagic flux by physically dissociating Beclin-1 from the Vps34–Vps15 complex independent of its kinase activity. Down-regulation of ErbB2 by CL-387,785 decreased the levels of C99 and secreted amyloid-β in cellular, zebrafish, and mouse models of AD, through the activation of autophagy. Oral administration of an ErbB2-targeted CL-387,785 for 3 wk significantly improves the cognitive functions of APP/presenilin-1 (PS1) transgenic mice. This work unveils a noncanonical function of ErbB2 in modulating autophagy and establishes ErbB2 as a therapeutic target for AD.

ErbB2 | Alzheimer's disease | Aβ | C99 | autophagy

Amyloid plaques are the primary cause of neurodegeneration in the brains of patients with Alzheimer's disease (AD) (1). Amyloid plaques are composed of amyloid-β (Aβ) peptides that are produced by stepwise cleavages of amyloid precursor protein (APP) by β- and γ-secretase (2). Therapeutic approaches toward treatment of AD developed in the past decade have centered on the prevention of Aβ production (3). The majority of these studies focused on either the augmentation of α-secretase activity, which can reduce the production of Aβ, or the inhibition of β-/γ-secretase activities (4). Unfortunately, the nonselective inhibition of β-secretase and γ-secretase results in unavoidable side effects due to the interference of other physiological substrates of β-secretase and γ-secretase (5, 6).

ErbB2 is a member of the epidermal growth factor receptor (EGFR)/ErbB family [which consists of four closely related receptor tyrosine kinases (ErbB1–4, also known as HER1–4)] and is tightly associated with neuritic plaques in AD (7). The correlation between EGFR/ErbB signaling and AD pathogenesis has been well documented in various studies (8–10). Ras GTPase activation mediates EGF-induced stimulation of γ-secretase to increase the nuclear function of the APP intracellular domain (AICD) (11). Consistent with the role of EGF signaling in AD, the intracellular mediators downstream of EGF signaling (which include Grb2, ShcA, and Abl) directly or indirectly interact with APP (12); these findings support the correlation between EGFR/ErbB-dependent signaling and AD susceptibility.

Autophagy controls the clearance of misfolded proteins and damaged organelles, and plays an essential role in maintaining neuronal functions (13, 14). Previous studies have demonstrated that autophagy is instrumental to the clearance of proteins related to neurodegenerative diseases; these proteins include polyglutamine aggregates in Huntington's disease, Lewy body-like α-synuclein aggregates in Parkinson's disease, and neurofibrillary tangles in AD (15–18). A previous study has shown that activated ErbB1 can inhibit autophagic flux to promote tumor progression and that inhibition of ErbB1 kinase can restore the autophagy activity to suppress tumor growth in lung cancer (19). By the same token, ErbB1 kinase inhibition by means of oral feeding of Gefitinib successfully alleviated memory impairment, but did not significantly alter Aβ load, in transgenic AD mice (20). However, whether further ErbB2 inhibition could increase autophagic flux remains elusive.

Recent studies have discovered a number of chemical and genetic γ-secretase modulators that can regulate Aβ production while exerting negligible effects on the γ-secretase–mediated processing of Notch (21–26). These findings thus warrant a systemic screen of novel genetic modifiers encoded in the human genome whose functions can selectively govern γ-secretase–mediated APP processing. We developed bioluminescence resonance energy transfer (BRET)-based cellular assays to systematically quantify the protein–protein interactions between γ-secretase and its substrates, either APP C-terminal fragment [APP-CTF; 99-residue CTF (C99)] or extracellular domain truncated Notch (NΔE), in response to the deficiency of a particular kinase or phosphatase encoded in the human genome. This RNA

Significance

We demonstrate that ErbB2 can regulate autophagic flux through its direct interaction with Beclin-1, which effectively blocks autophagy initiation. Although the expression of ErbB2 becomes dormant during adulthood, it becomes reactivated during the pathogenesis of Alzheimer's disease (AD), blocking the autophagy-mediated clearance of amyloid precursor protein (APP) C-terminal fragments (CTFs) [99-residue CTF (C99)]. Consequently, the accumulated APP-C99 can be further processed by γ-secretase, resulting in augmented production of amyloid-β and the APP intracellular domain. The chemical inhibition of ErbB2 by CL-387,785 effectively rescues the cognitive impairment of APP/presenilin-1 (PS1) transgenic AD mice. The present study thus defines a molecular basis by which the aberrant expression of ErbB2 could instigate the pathogenesis of AD. These findings provide the proof-of-principle evidence for rational design of ErbB2-targeted therapeutics for AD.

Author contributions: B.-J.W. and Y.-F.L. designed research; B.-J.W., Y.-W.C., and Y.-T.T. performed research; G.M.H., M.-K.H., W.-M.H., H.L., L.-W.J., S.-P.L.H., R.P.-Y.C., and C.-J.H. contributed new reagents/analytic tools; B.-J.W., G.M.H., P.-Y.W., and Y.-F.L. analyzed data; and B.-J.W. and Y.-F.L. wrote the paper.

The authors declare no conflict of interest.

This article is a PNAS Direct Submission.

[1]To whom correspondence should be addressed. Email: yliao@sinica.edu.tw.

This article contains supporting information online at www.pnas.org/lookup/suppl/doi:10.1073/pnas.1618804114/-/DCSupplemental.

interference (RNAi) screen led us to identify an ErbB2-interacting network that plays a critical role in governing the substrate availability of γ-secretase. Our findings provide direct evidence that inhibition of ErbB2 expression can enhance C99 clearance, thereby effectively decreasing Aβ production through activating autophagy. Our data further support the notion that defective autophagy is instrumental to proteinopathy-induced neurodegeneration. The present study also delineates an ErbB2-targeted therapeutic strategy (e.g., CL-387,785, an EGFR/ErbB2 inhibitor) that could render cognitive improvement without eliciting complications associated with undesirable Notch inhibition (e.g., γ-secretase inhibitors) for the next-generation treatment of AD.

Results

An shRNA Screen Identified Candidate Genes That Differentially Regulate the Proteolysis of APP-C99 and NΔE. We previously identified c-Jun N-terminal kinase and extracellular signal-regulated kinase as positive and negative regulators of γ-secretase activity, respectively (27, 28). We sought to determine whether additional kinases or phosphatases could differentially modulate the interaction between APP-C99 and presenilin-1 (PS1, the catalytic subunit of γ-secretase) without affecting the interaction between NΔE and PS1. We first established and validated cell-based BRET assays to measure the interactions between γ-secretase and its substrates quantitatively (Fig. 1 *A*–*D*). The specificity of these BRET assays can be confirmed by the introduction of an untagged protein partner to disrupt the targeted protein–protein interaction responsible for the BRET signal. Consistent with this notion, the expression of untagged PS1 or untagged nicastrin (NCT) can interfere with the interaction between *Renilla* luciferase (RL)-tagged PS1 (RL-PS1) and yellow fluorescent protein (YFP)-tagged NCT (NCT-YFP) (Fig. 1*A*), whereas untagged PS1 or Gal4VP16 (GV)-tagged C99 (C99-GV) can hinder the interaction between RL-PS1 and C99-YFP (Fig. 1*B*), and whereas untagged PS1 or untagged NΔE-GV can compete off the interaction between RL-PS1 and NΔE-YFP (Fig. 1*C*), to suppress the corresponding BRET signal. In a control cell line overexpressing RL-YFP fusion protein, which generates a constant BRET signal, untagged NCT, C99-GV, and NΔE cannot alter the RL-YFP–emitted BRET signal (Fig. 1*D*), further substantiating the specificity of the BRET signals corresponding to the PS1-NCT, PS1-C99, and PS1-NΔE interactions. These BRET cell lines were then subjected to RNAi screens with the human kinase and phosphatase subset, which contains 5,667 validated shRNA-encoding lentiviral clones targeting 777 human kinases and 237 human phosphatases (*SI Materials and Methods* and Dataset S1). If the targeted gene is involved in modulating the interaction of PS1-C99 or PS1-NΔE, its down-regulation would reduce the BRET signal. By selecting those genes whose down-regulation resulted in a decrease greater than 20% in PS1-C99–elicited BRET signal and changes less than 20% in PS1-NCT–elicited and PS1-NΔE–elicited BRET signals, we identified 44 candidate genes that preferentially influence the interaction of PS1 and C99. Further analysis using STRING software [version 10 (29)] at the highest stringency (0.9 confidence index) to highlight the interconnected signaling transducers that are involved in the regulation of γ-secretase substrate selectivity, a subnetwork of 14 genes was identified for experimental confirmation (Fig. 1*E* and Datasets S2 and S3). ErbB2 was chosen to be further validated for its role in the pathogenesis of AD primarily due to its multiple connections to other candidate genes in this network and the wealth of available chemical inhibitors. The biochemical characteristics associated with ErbB2 thus made it an appealing target for the translational study to determine the underlying mechanism.

The Expression Levels of ErbB2 Are Significantly Elevated in AD Brains. To correlate the ErbB2-elicited regulation of γ-secretase with AD pathogenesis, we examined the levels of ErbB2 in brain homogenates derived from either normal individuals or patients with sporadic AD. Significantly higher levels of ErbB2 expression in hippocampal regions of patients with AD were observed compared with aged-matched normal controls, whereas the levels of EGFR exhibited no significant difference between AD brain and age-matched control brain samples (Fig. 2 *A* and *B*). Furthermore, the levels of ErbB2 in whole-brain homogenates were significantly higher in newborn mice than in young (3-mo-old) and old (15-mo-old) mice (Fig. 2*C*). Consistently, the expression of ErbB2 in human brain was gradually decreased with increasing age (Fig. 2*D*). Our data were thus in line with the notion that the expression of ErbB2 is abundant during the embryonic development of both the central and peripheral nervous systems and gradually declines in adult human brain (Human Protein Atlas, www.proteinatlas.org) (30, 31). These preliminary results suggest that the recurring ErbB2 in aged brain could be a disease-driving instigator for sporadic AD.

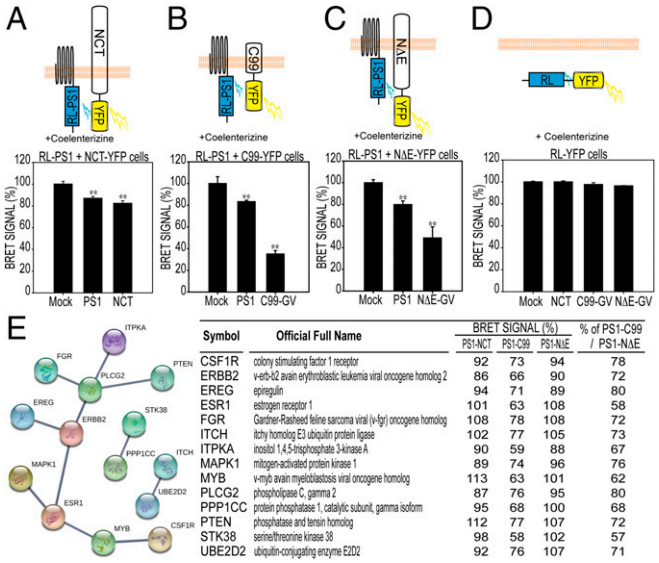

Symbol	Official Full Name	BRET SIGNAL (%) PS1-NCT	PS1-C99	PS1-NΔE	% of PS1-C99 / PS1-NΔE
CSF1R	colony stimulating factor 1 receptor	92	73	94	78
ERBB2	v-erb-b2 avain erythroblastic leukemia viral oncogene homolog 2	86	66	90	72
EREG	epiregulin	94	71	89	80
ESR1	estrogen receptor 1	101	63	108	58
FGR	Gardner-Rasheed feline sarcoma viral (v-fgr) oncogene homolog	108	78	108	72
ITCH	itchy homolog E3 ubiquitin protein ligase	102	77	105	73
ITPKA	inositol 1,4,5-trisphosphate 3-kinase A	90	59	88	67
MAPK1	mitogen-activated protein kinase 1	89	74	96	76
MYB	v-myb avain myeloblastosis viral oncogene homolog	113	63	101	62
PLCG2	phospholipase C, gamma 2	87	76	95	80
PPP1CC	protein phosphatase 1, catalytic subunit, gamma isoform	95	68	100	68
PTEN	phosphatase and tensin homolog	112	77	107	72
STK38	serine/threonine kinase 38	98	58	102	57
UBE2D2	ubiquitin-conjugating enzyme E2D2	92	76	107	71

Fig. 1. shRNA screens for identifying genetic modifiers that govern the protein–protein interaction of PS1-NCT, PS1-C99, and PS1-NΔE. The generation of cell-based BRET assays for detecting the interactions of PS1-NCT, PS1-C99, and PS1-NΔE is described in *Materials and Methods*. The specificity of BRET cells was determined by transiently transfecting cells with an empty vector (Mock), untagged PS1, untagged NCT, C99-GV, or NΔE-GV to compete in protein–protein interaction. (*A*) Specificity of PS1-NCT-BRET cells. (*B*) Specificity of PS1-C99-BRET cells. (*C*) Specificity of PS1-NΔE-BRET cells. (*D*) Positive BRET control cells that express the RL-tagged YFP fusion protein were transiently transfected with an empty vector, untagged NCT, C99-GV, or NΔE-GV. Data are shown as the mean ± SD from three independent experiments, and were analyzed by Student's *t* tests. $^{**}P < 0.01$. (*E*) PS1-C99-BRET cells and PS1-NΔE-BRET cells were subjected to shRNA screens. Candidate genes were identified based on their differential effects on the BRET signals of PS1-C99-BRET, PS1-NΔE-BRET, and PS1-NCT-BRET cells. Analysis using STRING software resulted in the identification of 14 connected genes that preferentially affect the interaction between PS1 and C99.

Inhibition of ErbB2 by CL-387,785 Can Differentially Promote the Clearance of C99 Without Affecting Notch Signaling. To examine the substrate-specific γ-secretase cleavages, we generated a HEK293-derived cell line (CG) that was stably cotransfected with a tetracycline-inducible C-terminally Gal4/VP16-tagged C99 and a Gal4 promoter-driven luciferase reporter gene. We also generated another HEK293-derived cell line (NG) that was stably cotransfected with a tetracycline-inducible C-terminally Gal4/VP16-tagged NΔE and a Gal4 promoter-driven luciferase reporter gene (Fig. 3*A*). Both the CG and NG cell lines exhibited decreased γ-secretase–dependent luciferase signals in the presence

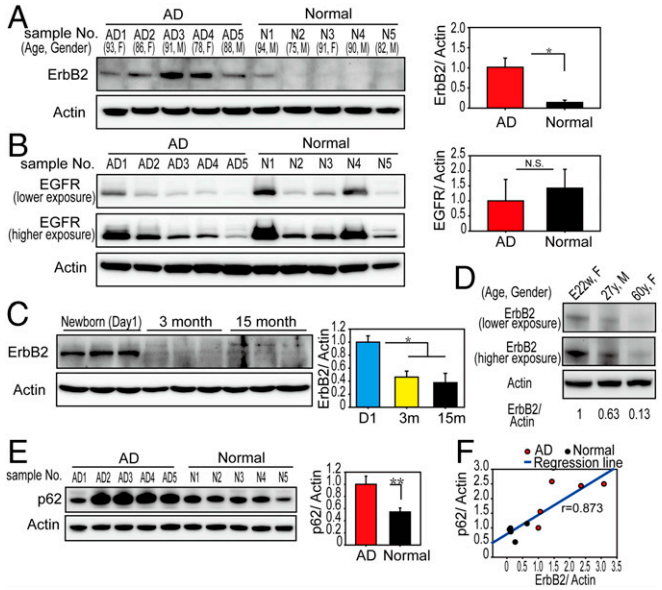

Fig. 2. Levels of ErbB2 are positively correlated with age-related sporadic AD, but are reduced in normal adult mouse and human brain. (*A* and *B*) Human hippocampal regions were analyzed by Western blotting with anti-EGFR(ErbB1), anti-ErbB2, and anti-actin antibodies. $*P < 0.05$. N.S., not significant. (*C*) Mouse whole-brain lysates were examined by Western blotting with anti-ErbB2 and anti-actin antibodies. The levels of EGFR and ErbB2 were normalized with the level of actin. The quantitative data are shown as the mean ± SEM, and were analyzed by Student's *t* tests. $*P < 0.05$. (*D*) Human whole-brain lysates were analyzed by Western blotting with anti-ErbB2 and anti-actin antibodies. The age and gender of the individuals whose brain homogenates were derived are denoted. F, female; M, male. (*E*) Human hippocampal regions were analyzed by Western blotting with anti-p62 antibody. The quantitative data of p62 are shown as the mean ± SEM, and were analyzed by Student's *t* tests. $**P < 0.01$. (*F*) Correlation between the levels of p62 and ErbB2 was calculated by Pearson's correlation.

of *N*-[*N*-(3,5-difluorophenacetyl-L-alanyl)]-S-phenylglycine t-butyl ester (DAPT), a known γ-secretase inhibitor, in a dose-dependent manner (Fig. S1 *A* and *B*), suggesting that γ-secretase in CG and NG cells exhibited comparable catalytic properties.

To determine whether ErbB1 or ErbB2 receptor tyrosine kinase activity is essential for the differential modulation of C99 cleavage, we first examined the luminescence signals in CG and NG cells treated with various ErbB1/2 inhibitors. Our data showed that only CL-387,785 (ErbB1/2 dual), but not AG825 (ErbB2-selective), Gefitinib (ErbB1-selective), or Lapatinib (ErbB1/2 dual), effectively blocked the processing of C99 (in CG cells), but not NΔE (in NG cells) (Fig. 3*B* and Fig. S1 *C*–*J*). Furthermore, using C99-YFP–overexpressing HEK293 cells, we found that treatments with CL-387,785 concomitantly decreased the levels of ErbB2, C99, and AICD (Fig. 3*C*).

To address how ErbB1 and ErbB2 could act in a differential mode upon the coexistence of C99 and NΔE, we generated a HEK293 cell line that stably coexpressed ErbB1, ErbB2, cyan fluorescent protein (CFP)-tagged C99, and YFP-tagged NΔE. Consistently, ErbB2 knockdown, but not ErbB1 knockdown, was sufficient to induce a concomitant reduction in the levels of C99 and AICD (Fig. 3*D*). This finding was further confirmed with the data that RNAi-mediated down-regulation of ErbB2 resulted in a selective decrease in C99 signaling (CG cells), but not Notch signaling (NG cells), phenocopying CL-387,785–induced effects (Fig. 3 *E* versus *B*). Furthermore, HEK293 cells that are cotransfected with YFP-tagged C99 and His-tagged ErbB2 exhibited a significant accumulation of C99 and AICD compared with the mock-transfected cells (Fig. 3*F*). However, both the overexpression and down-regulation of ErbB1 can induce a concomitant accumulation of C99 and AICD (Fig. 3 *D* and *F*), suggesting that the reduction of C99 and AICD by CL-387,785 might not be transduced through ErbB1. Given that treatments with CL-387,785 primarily result in a very selective decrease in the protein level of ErbB2, but not ErbB1 (Fig. 3*C*), and that only ErbB2 knockdown can phenocopy the effect of CL-387,785, our findings strongly favor a model in which ErbB2 modulates the availability of C99 and AICD.

Depletion of ErbB2 Promotes the Autophagic Clearance of C99 and AICD. We previously proposed that autophagy plays a central role in the maintenance of intracellular Aβ production (14). We hypothesized that ErbB2 may affect the autophagic clearance of intracellular C99 and AICD. To confirm the ErbB2-mediated modulation of autophagy, we examined the ErbB2-induced accumulation of C99 and AICD in response to RNAi down-regulation of autophagy-related 5 (ATG5) gene, an essential component for the elongation and formation of autophagosomes (32). ATG5 also forms a multimeric complex with ATG12 and ATG16 to mediate the lipidation of microtubule-associated protein 1A/1B light chain 3 (LC3) and the membrane tethering of LC3 onto the surface of autophagosomes (13). The conversion of cytosolic LC3 (LC3-I) to lipidated and membrane-bound LC3 (LC3-II), along with the appearance of LC3 puncta, has been characterized to be the marker for autophagosomes and molecular indicators of autophagy induction (13). Using HEK293 cells that overexpressed ErbB1, ErbB2, CFP-tagged C99, and YFP-tagged NΔE, we demonstrated that the reduction in C99 and AICD elicited by ErbB2 knockdown could be rescued by concurrent down-regulation of ATG5 (Fig. 4*A*). Furthermore, using a CFP-LC3–overexpressing HEK293 cell line, we found that ErbB2 knockdown induced significant accumulation of CFP-LC3 puncta, whereas the short hairpin ErbB2 (shErbB2)-induced formation of CFP-LC3 puncta was blocked by ATG5 knockdown (Fig. 4 *B* and *C*). Consistently, ErbB2 down-regulation increased LC3-II production, which can be reversed by concurrent ATG5 knockdown (Fig. 4*D*). Together, our data suggest a novel role of ErbB2 in modulating autophagy.

We then sought to distinguish the potential cross-talk between ErbB2 and ErbB1 in modulating autophagy, given that ErbB2 forms heterodimers with ErbB1. Using a HEK293 cell line that stably overexpressed ErbB1, ErbB2, CFP-tagged C99, and YFP-tagged NΔE, we determined the levels of sequestosome-1/p62 and LC3-I/II in response to either ErbB1 or ErbB2 knockdown. Accumulated evidence has demonstrated that p62 is a cargo receptor protein that delivers ubiquitinated substrates and misfolded proteins for autophagic clearance through its interaction with LC3 (33). Inhibition of autophagy can thus lead to a significant accumulation of p62 and a decrease in the LC3-II/I ratio, two phenotypic abnormalities commonly seen in degenerating neurons in AD and related neurodegenerative diseases (33, 34). Our data showed that although down-regulation of ErbB1 resulted in significant accumulation of p62 and an increase in the LC3-II/I ratio, depletion of ErbB2 caused a significant reduction in p62 with a concomitant increase in the LC3-II/I ratio (Fig. 4*E*), suggesting that inhibition of ErbB2 is sufficient to induce autophagy. Interestingly, despite the accumulation of C99 and AICD caused by RNAi-mediated down-regulation of ErbB1 (Fig. 3*D*), suppression of ErbB1 can still effectively decrease Aβ40 production (Fig. 4*F*). More importantly, down-regulation of ErbB2 had a much stronger impact than down-regulation of ErbB1 on the production of secreted Aβ40 (Fig. 4*F*). In HEK293 cells that overexpressed C99-YFP, treatments with CL-387,785 led to a significant reduction in p62 and a concurrent increase in the LC3-II/LC3-I ratio (Fig. 4*G*), indicative of autophagy induction. Consistent with the effect induced by ErbB2 knockdown, depletion of ErbB2 by CL-387,785 effectively decreased secreted Aβ40 production (Fig. 4*H*). Together, these results point toward a novel ErbB2-dependent pathway that governs the autophagic clearance of APP-C99 to modulate Aβ production.

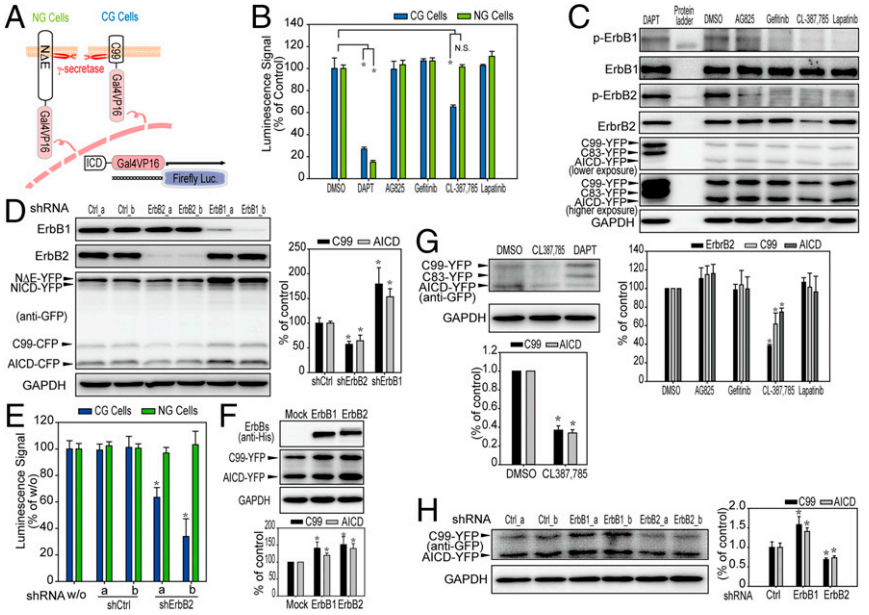

Fig. 3. Alterations in the levels of ErbB1 and ErbB2 can reciprocally govern the steady-state levels of C99/AICD and NΔE/Notch intracellular domain. The generation of cell-based assays for detecting γ-secretase activity is described in *Materials and Methods*. (*A*) Characterization of APP-C99–based (CG) and NΔE-based (NG) γ-secretase assays. Luc, luciferase. (*B*) Adherent CG and NG cells (20,000 cells per well) were treated with 1 μM ErbB1/2-selective tyrosine kinase inhibitors, as indicated, in the presence of 1 μg/mL tetracycline at 37 °C for 24 h. The luminescence signals emitted by cells treated with vehicle alone (0.1% DMSO) were referred to as 100% relative luminescence signals. The luminescence signals generated by γ-secretase–mediated proteolysis of C99 (CG) or NΔE (NG) were determined using the Steady-Glo luciferase assay reagent. (*C*) HEK293-overexpressing C99-YFP cells were treated with 1 μM ErbB1/2 tyrosine kinase inhibitors, as indicated, at 37 °C for 24 h. Clarified lysates were analyzed by Western blotting and quantified by ImageJ (NIH). (*D*) HEK293-overexpressing ErbB1, ErbB2, CFP-tagged C99, and YFP-tagged NΔE cells were infected with gene-targeting shRNA-encoding lentivirus (shErbB1 or shErbB2) at 37 °C for 48 h. Clarified lysates containing equivalent amounts of proteins were examined by Western blotting and quantified by ImageJ. Ctrl, control; NICD, Notch intracellular domain. (*E*) CG and NG cells were infected with gene-targeting shRNA-encoding lentivirus at 37 °C for 48 h following induction with 1 μg/mL tetracycline for 24 h. Cells infected with empty lentivirus (w/o) or LacZ-targeting shRNA lentivirus (shCtrl_a and shCtrl_b) were included as controls. Data are shown as the mean ± SD from three independent experiments, and were analyzed by Student's *t* tests. $*P < 0.05$. (*F*) HEK293 cells overexpressing C99-YFP were infected with control lentivirus or lentivirus encoding either His-tagged ErbB1 or His-tagged ErbB2 at 37 °C for 72 h, and were then analyzed by Western blotting with anti-GFP antibody to visualize the levels of C99-YFP and AICD-YFP simultaneously. Data are shown as the mean ± SD from three independent experiments, and were analyzed by Student's *t* tests. $*P < 0.05$. (*G*) IMR32 cells overexpressing C99-YFP were grown with 2 mL of fresh culture medium in six-well plates and treated with 1 μM CL-387,785 or DAPT at 37 °C for 24 h. The cell extracts were analyzed by Western blotting. (*H*) C99-YFP–expressing IMR32 cells (160,000 cells per well) were seeded onto six-well plates and cultured at 37 °C for 24 h, and then infected with ErbB1- or ErbB2-targeting shRNA lentivirus for an additional 48 h. Infection mixtures were replaced with 2 mL of fresh culture medium, and infected cells were then incubated at 37 °C for an additional 24 h. The cell extracts were analyzed by Western blotting with anti-GFP antibody.

Inhibition of ErbB2 Significantly Alleviates the Production of C99 and AICD in Neuroblastoma Cells. To substantiate the critical role of ErbB2 in the homeostasis of APP processing and Aβ production, we examined the level of secreted Aβ40 in conditioned media derived from cells treated with CL-387,785 or infected with lentiviral vectors encoding either ErbB1- or ErbB2-targeting shRNAs. Chemical depletion of ErbB2 by CL-387,785 significantly reduced the levels of C99, AICD, and secreted Aβ40 in IMR32 neuroblastoma cells overexpressing C99-YFP (Figs. 3*G* and 4*J*). These findings were further confirmed by the data that RNAi-mediated down-regulation of ErbB2 (shErbB2) significantly reduced the levels of C99, AICD, and secreted Aβ40 in C99-YFP–expressing IMR32 cells, whereas ErbB1 knockdown (shErbB1) induced a slight increase in the accumulation of C99 and AICD but a marginal reduction in Aβ40 (Figs. 3*H* and 4*K*).

ErbB2 Interferes with the Formation of the Beclin-1–Vps34–Vps15 Complex. A great number of studies have previously demonstrated that the Beclin-1–Vps34–Vps15 multimeric complex can govern the nucleation of autophagy, as evidenced by the increased interaction between Beclin-1 and the Vps34–Vps15 complex in response to either starvation or rapamycin treatments (19, 35, 36). Given that Beclin-1 has been shown to interact physically with ErbB2 (37), we thus reasoned that ErbB2 could bind to Beclin-1 and modulate the autophagic flux to control the autophagic clearance of C99 and AICD. To determine the molecular mechanism underlying the ErbB2-mediated regulation of autophagic flux, we examined the interaction between ErbB2 and Beclin-1 and the formation of the Beclin-1–Vps34–Vps15 complex, along with the levels of p62 and LC3-I/II, in the presence or absence of rapamycin. Consistent with the finding that ErbB2 acts as a negative regulator of autophagy, overexpression of ErbB2 in HEK293 cells caused p62 accumulation and decreased autophagic flux (LC3-II/I ratio) (Fig. 4*I*). When treated with rapamycin, ErbB2-overexpressing HEK293 cells exhibited inefficient p62 degradation and a lower LC3-II/I ratio compared with the rapamycin-treated, mock-transfected control (Fig. 4*I*). These findings suggest that overexpression of ErbB2 can withstand the initiation of rapamycin-induced autophagy. Consistent with this notion, endogenous ErbB2 in HEK293 cells associated with Beclin-1 in the basal state as well as in the rapamycin-treated state, whereas there was no detectable interaction between EGFR and Beclin-1 in the presence or absence of rapamycin (Fig. 5*A*). Moreover, ErbB2 knockdown can strengthen the interaction between Beclin-1 and the Vps34–Vps15 complex (Fig. 5*B*), suggesting that ErbB2 may act as a gatekeeper for the formation of the Beclin-1–Vps34–Vps15 complex to maintain the autophagic flux at a basal state. It was previously reported that expression of N-terminally truncated ErB2 (ErbB2ΔE) can render autophagy-induced apoptosis (38, 39). We also found that

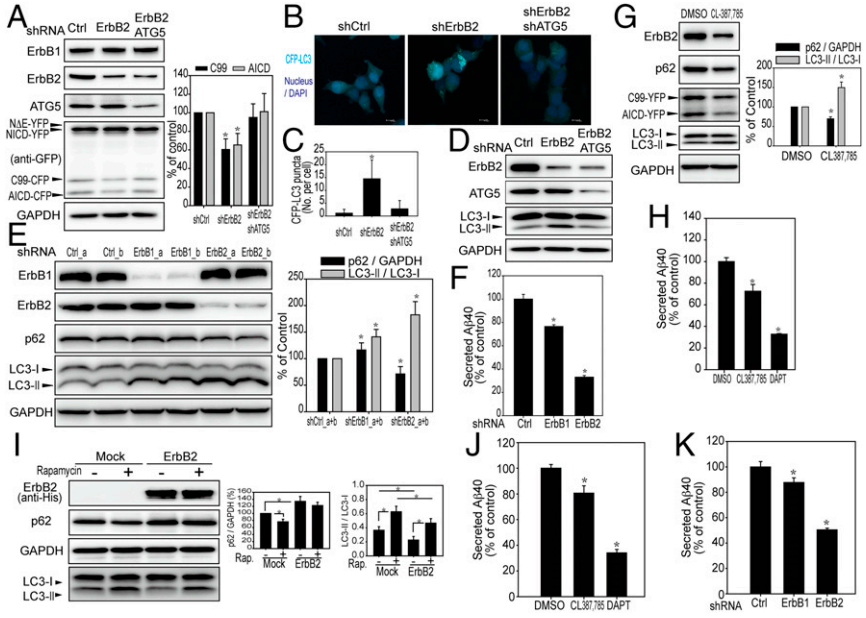

Fig. 4. ErbB2 controls the proteostasis of C99 and AICD through the autophagy-lysosomal pathway. (*A*) HEK293 cells coexpressing ErbB1, ErbB2, CFP-tagged C99, and YFP-tagged NΔE were infected with lentivirus encoding shRNA targeting LacZ (Ctrl), ErbB2, or ErbB2 plus ATG5 for 48 h. Clarified lysates containing equivalent amounts of proteins were analyzed by Western blotting. The quantitative data are shown as the mean ± SD from three independent experiments, and were analyzed by Student's *t* tests. $*P < 0.05$. (*B–D*) HEK293 cells overexpressing CFP-LC3 were infected with lentivirus encoding shRNA targeting LacZ (Ctrl), ErbB2, or ErbB2 plus ATG5 for 48 h. The autophagy induction was analyzed by fluorescence confocal microscopy. The number of CFP-LC3 puncta per cell was quantified. The levels of LC3-I, LC3-II, and GAPDH were analyzed by Western blotting. (Scale bar, 10 μm.) (*E* and *F*) HEK293 cells overexpressing ErbB1, ErbB2, CFP-tagged C99, and YFP-tagged NΔE were infected with lentivirus encoding shRNA targeting LacZ (Ctrl), ErbB1, or ErbB2 for 48 h. Infection mixtures were replaced with 2 mL of fresh culture medium, and infected cells were then incubated at 37 °C for an additional 24 h. The levels of LC3-I, LC3-II, and p62 were analyzed by Western blotting and quantified by ImageJ (66). Conditional media were harvested and processed for determination of secreted Aβ40 using a colorimetric Aβ40-specific ELISA kit. (*G* and *H*) HEK293 cells overexpressing C99-YFP were treated with vehicle (DMSO) or 1 μM CL-387,785 at 37 °C for 24 h and analyzed by Western blotting. Conditional media were harvested for determination of secreted Aβ40. The quantitative data are shown as the mean ± SD from three independent experiments, and were analyzed by Student's *t* tests. $*P < 0.05$. (*I*) HEK293 cells were infected with control lentivirus (Ctrl) or lentivirus encoding 6× His-tagged ErbB2 and then treated with vehicle (DMSO) or 200 nM rapamycin at 37 °C for 3 h. Clarified lysates containing equal amounts of proteins were analyzed by Western blotting and quantified by ImageJ. The quantitative data are shown as the mean ± SD from three independent experiments, and were analyzed by Student's *t* tests. $*P < 0.05$. (*J*) IMR32 cells overexpressing C99-YFP were grown with 2 mL of fresh culture medium in six-well plates, and treated with 1 μM CL-387,785 or DAPT at 37 °C for 24 h. Conditional media were harvested and processed for determination of secreted Aβ40 using a colorimetric Aβ40-specific ELISA kit. (*K*) C99-YFP–expressing IMR32 cells (160,000 cells per well) were seeded onto six-well plates and cultured at 37 °C for 24 h, and then infected with ErbB1- or ErbB2-targeting shRNA lentivirus for an additional 48 h. Infection mixtures were replaced with 2 mL of fresh culture medium, and infected cells were then incubated at 37 °C for an additional 24 h. The conditioned media were harvested and processed for determination of secreted Aβ40. Data are the mean ± SD from three independent experiments, and were analyzed by Student's *t* tests. $*P < 0.05$.

in HEK293 cells overexpressing FLAG-tagged Beclin-1, overexpression of constitutively active ErbB2ΔE resulted in even greater attenuation in the binding of Beclin-1 to the Vps34–Vps15 complex than wild-type ErbB2 (wtErbB2) did (Fig. 5*C*). The ErbB2–Beclin-1 complex did not contain Vps34–Vps15 (Fig. 5*D*), suggesting that overexpression of ErbB2 can disrupt the assembly of autophagy initiation complexes. This notion was corroborated by the observation that overexpression of ErbB2ΔE resulted in a greater accumulation of C99 and AICD than wtErbB2 did in C99-YFP–expressing HEK293 cells (Fig. 5*E*). Using fluorescence confocal microscopy, we further demonstrated that wtErbB2 and mutant ErbB2ΔE are colocalized with Beclin-1 at the basal state (Fig. 5*F*). Together, our data suggest that ErbB2 actively governs autophagic flux through limiting the availability of Beclin-1 to the Vps34–Vps15 complex.

Monomeric and Kinase-Dead ErbB2 Can Interact with Beclin-1. To determine whether the ErbB2 kinase activity is required for its role in the regulation of autophagic flux, we examined the interaction between Beclin-1 and the Vps34–Vps14 complex in response to the overexpression of wtErbB2 or a kinase-dead (KD) mutant ErbB2 (K753M). HEK293 cells overexpressing wtErbB2 or KD-ErbB2 (K753M) exhibited comparable binding with Beclin-1, suggesting that the binding of ErbB2 with Beclin-1 is kinase-independent (Fig. 6*A*). To verify the physical interaction between ErbB2 and Beclin-1 further and to rule out the potential involvement of other ErbB isoforms, we used CHO-K1 cells that do not express ErbB1, ErbB3, or ErbB4 for further studies (40). Overexpression of wtErbB2 or a KD and monomeric mutant ErbB2 [ErbB2-VVI/AAA(966–968) (41)] in CHO-K1 cells was induced, and the interaction with Beclin-1 was analyzed by coimmunoprecipitation using anti–Beclin-1 antibody. We found that monomeric mutant ErbB2-VVI/AAA binds to Beclin-1 and attenuates Beclin-1's association with the Vps34–Vps15 complex as effectively as wtErbB2 does (Fig. 6 *B–D*). Consistently, overexpression of ErbB2-VVI/AAA in C99-YFP–expressing HEK293 cells caused a significant accumulation of C99 and AICD comparable to what wtErbB2 did (Fig. 6*E*). These data unequivocally suggest that monomeric ErbB2 is sufficient to bind Beclin-1 and regulate the autophagic flux in a kinase-independent manner.

CL-387,785 Treatments Significantly Reduce the Levels of C99 and AICD in a Zebrafish Model of Amyloidopathy. To determine whether ErbB2 mediates selective modulation of the proteostasis of C99 in vivo, we generated a zebrafish model of amyloidopathy, in which embryos express green fluorescent protein (GFP)-tagged C99 (Fig. 7*A*). Previous studies have used zebrafish as an in vivo model to validate the biological efficacy of Aβ-lowering drugs, and attribute the drug-elicited developmental defects on somitogenesis to attenuated Notch signaling (42). The expression of GFP-tagged C99 was driven by cytomegalovirus promoter and a

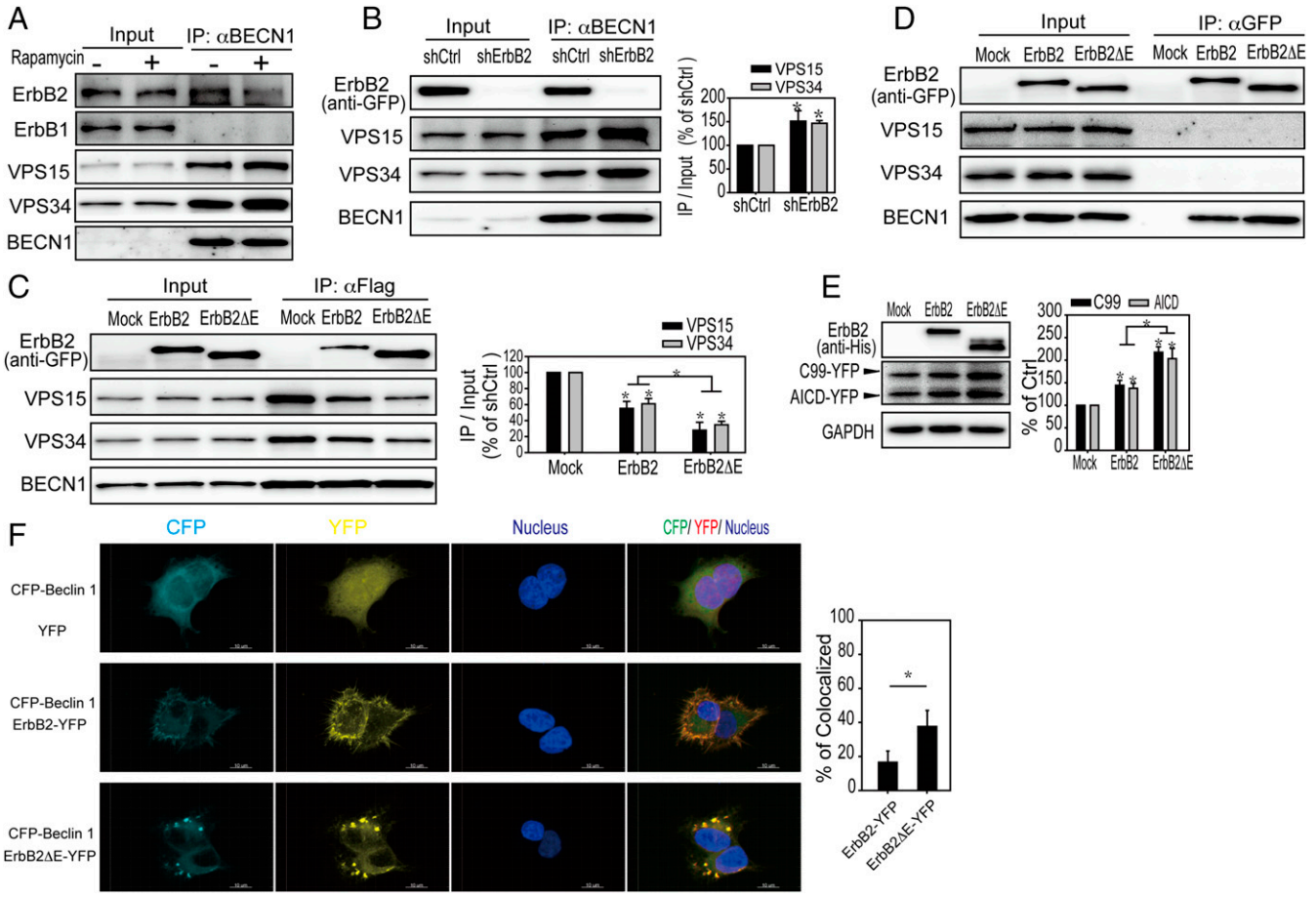

Fig. 5. ErbB2 physically interacts with Beclin-1 and disrupts the formation of the tripartite Beclin-1–Vps34–Vps15 complex. (*A*) HEK293 cells were treated with vehicle (DMSO) or 200 nM rapamycin at 37 °C for 3 h. Clarified lysates were immunoprecipitated with anti–Beclin-1 antibody (αBECN1). Immobilized proteins were analyzed by Western blotting with anti-ErbB1, anti-ErbB2, anti-Vps15, anti-Vps34, and anti–Beclin-1 antibodies. IP, immunoprecipitation. (*B*) HEK293 cells overexpressing YFP-tagged ErbB2 were infected with lentivirus encoding shRNA targeting LacZ (Ctrl) or ErbB2 (shErbB2) at 37 °C for 72 h. Clarified lysates with equal amounts of proteins were subjected to immunoprecipitation with αBECN1. Immobilized proteins were analyzed by Western blotting with anti-ErbB2, anti-Vps15, anti-Vps34, and anti–Beclin-1 antibodies. The quantitative data are shown as the mean ± SD from three independent experiments, and were analyzed by Student's *t* tests. $*P < 0.05$. (*C* and *D*) HEK293 cells expressing FLAG–Beclin-1 were infected with control lentivirus (Ctrl) or virus encoding either YFP-tagged ErbB2 or YFP-tagged ErbB2-ΔE. Clarified lysates were then immunoprecipitated with anti-FLAG (*C*, αFlag) or anti-GFP (*D*, αGFP) antibody. The quantitative data in *C* are shown as the mean ± SD from three independent experiments, and were analyzed by two-way ANOVA. $*P < 0.05$. (*E*) HEK293 cells expressing C99-YFP were infected with control lentivirus (Ctrl) or lentivirus encoding either His-tagged ErbB2 or His-tagged ErbB2ΔE at 37 °C for 72 h, and were then analyzed by Western blotting and quantified by ImageJ. The quantitative data are shown as the mean± SD from three independent experiments, and were analyzed by two-way ANOVA. $*P < 0.05$. (*F*) HEK293 cells overexpressing CFP–Beclin-1 were infected with control lentivirus (Ctrl) or lentivirus encoding YFP, YFP-tagged ErbB2, or YFP-tagged ErbB2ΔE at 37 ° for 72 h, and were visualized by fluorescence confocal microscopy to determine expression and localization. Approximately 100 cells of each group were analyzed by Imaris 3D software to measure the percentage of colocalization between CFP–Beclin-1 and recombinant ErbB2-YFP (wt or mutant), and then analyzed by two-way ANOVA. $*P < 0.05$. (Scale bar, 10 μm.)

flanking human β-globin chimeric intron. The coexpression of p2A-GFP fusion protein was used as an injection and expression control. Using this C99-expressing zebrafish model of amyloidopathy, we found that embryos treated with CL-387,785 exhibited a concomitant clearance of C99 and AICD (Fig. 7*B*). Consistent with previous findings, we also observed severe developmental defects in DAPT-treated zebrafish embryos, as evidenced by a curved trunk due to the concomitant blockade of Notch signaling by pan-inhibition of γ-secretase (43). In stark contrast to the DAPT-treated zebrafish embryos, CL-387,785–treated embryos exhibited normal somite development with wild-type trunks and tails (Fig. 7*C*), suggesting that Notch signaling-dependent somitogenesis is not affected by CL-387,785 treatment. These findings suggest that preferential depletion of C99 by CL-387,785 could be developed further as a novel therapeutic approach for AD with minimal side effects.

Inhibition of ErbB2 Significantly Alleviates the Production of Aβ and Renders Cognitive Improvement in APP/PS1 Transgenic Mice. To correlate the increased level of ErbB2 with defective autophagy in AD brain, we validated that lysates derived from the hippocampus regions of patients with AD contain a significantly increased accumulation of autophagic cargo receptor p62 compared with age-matched controls (Fig. 2*E*), suggesting that ErbB2-triggered autophagic deficiency is tightly associated with AD pathogenesis (Fig. 2 *A* and *F*). We further confirmed the biological efficacy of CL-387,785 on a murine model of AD. The dosing regimen of CL-387,785 (5 $mg \cdot kg \cdot d^{-1}$) did not induce any significant adverse effects on those APP*swe*/PS1ΔE9 double-transgenic mice, as evidenced by no significant difference in the body weight of animals treated with CL-387,785 or vehicle alone (Fig. S2). Treated APP*swe*/PS1ΔE9 transgenic mice, along with their wild-type littermates, were subjected to spatial learning and memory testing by the Morris water maze after 11 d of daily dosing. We found that

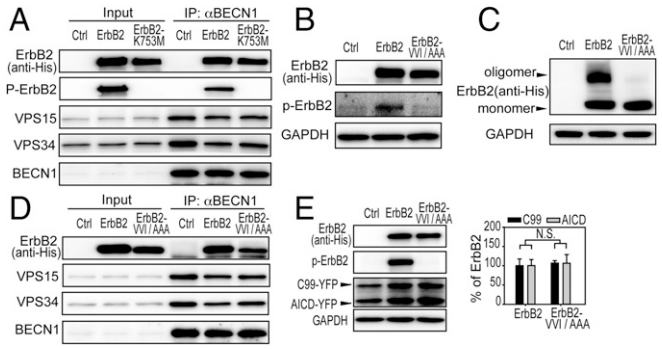

Fig. 6. Monomeric and oligomeric ErbB2 binds to Beclin-1 independent of its kinase activity. (*A*) HEK293 cells were infected with control lentivirus (Ctrl) or lentivirus encoding either His-tagged ErbB2 or His-tagged ErbB2-K753M, and were then immunoprecipitated with αBECN1. (*B*) CHO-K1 cells were infected with control lentivirus (Ctrl) or lentivirus encoding either His-tagged ErbB2 or His-tagged ErbB2-VVI/AAA(966–968). Clarified cell lysates were analyzed by Western blotting using anti-His (for ErbB2), anti–phospho-HER2/ErbB2 (Tyr1248), and anti-GAPDH. (*C*) Clarified lysates derived from infected CHO-K1 cells expressing ErbB2 or ErbB2-VVI/AAA were incubated with a cross-linker [bis(sulfosuccinimidyl)suberate, 1 mM; Thermo Fisher Scientific] at room temperature for 2 h, and were then analyzed by Western blotting with anti-His antibody (for ErbB2). These results confirmed that the mutant ErbB2 (ErbB2-VVI/AAA) exists as a monomeric form and lacks kinase activity. (*D*) CHO-K1 cells were infected with control lentivirus (Ctrl) or lentivirus encoding either His-tagged ErbB2 or His-tagged ErbB2-VVI/AAA (966–968), and were then immunoprecipitated with αBECN1, followed by Western blotting with antibodies against Beclin-1, Vps34, Vps15, and His tag. (*E*) HEK293 cells overexpressing C99-YFP were infected with control lentivirus (Ctrl) or lentivirus encoding either His-tagged ErbB2 or His-tagged ErbB2-VVI/AAA at 37 °C for 72 h, and were then analyzed by Western blotting. Clarified lysates containing equal amounts of proteins were analyzed by Western blotting and quantified by ImageJ. The quantitative data are shown as the mean ± SD from three independent experiments, and were analyzed by Student's *t* tests. $^*P < 0.05$.

APP*swe*/PS1ΔE9 transgenic mice administered with CL-387,785 exhibited significantly enhanced spatial learning after 16 d of daily dosing (Fig. 8*A*). After 3 wk of daily dosing, AD mice treated with CL-387,785 exhibited a dramatic cognitive improvement compared with vehicle-treated AD mice on the probe test with an invisible platform (Fig. 8*B*). Western blotting analysis of the brain homogenates of these APP*swe*/PS1ΔE9 transgenic mice further revealed that treatments with CL-387,785 induced a significant reduction in the levels of ErbB2, p62, and APP-CTF, concomitant with an increase in the ratio of LC3-II to LC3-I and a steady level of total APP (Fig. 8 *C* and *D*). Using coimmunoprecipitation, we verified that treatments with CL-387,785 in APP*swe*/PS1ΔE9 mice inhibited the phosphorylation of EGFR(ErbB1), and drastically suppressed the interaction between ErbB2 and Beclin-1 (Fig. 8 *E* and *F*), consistent with its effect on restoring autophagic flux. Most importantly, APP*swe*/PS1ΔE9 mice treated with CL-387,785 exhibited an ∼40% reduction in the levels of Aβ40 and Aβ42 in the brain (Fig. 8*G*). Collectively, we were able to confirm the molecular mechanism underlying the ErbB2-mediated regulation of autophagy using a number of cellular models that specifically address the delicate nature of protein–protein interactions involved in the ErbB2-modulated autophagic clearance of C99 and AICD. The mechanistic evidence was further validated in human brain tissues, a zebrafish model of amyloidopathy, and an APP/PS1 transgenic mouse model of AD, which is essential for us to be able to correlate our findings to the disease processes in human AD samples and to evaluate the biological efficacy of a selected drug candidate for its potential in clinical applications. Our findings thus unveil a noncanonical function of ErbB2 in the regulation of autophagic flux that contributes to the proteostasis of APP-C99, and thereby identify a therapeutic target for the development of anti-AD drugs with minimal side effects.

Discussion

The "amyloid cascade hypothesis," which states that the extracellular deposition of Aβ in the brain of patients with AD initiates the pathogenic cascade leading up to full-blown neurodegeneration, has been dominant in AD research as the primary etiological scenario occurring in AD brain for the past 25 y (1, 44, 45). Enormous efforts have been invested in finding effective disease-modifying cures for AD by alleviating Aβ-elicited neurotoxicity, but to no avail. A recent report showcased results from a phase 1b trial of aducanumab immunotherapy demonstrating that patients with prodromal or mild AD exhibit a positive outcome in cognition assessments after being treated with aducanumab for 1 y (46). The promising outcomes from aducanumab immunotherapy again support the notion that Aβ neurotoxicity likely plays a critical role in the early stage of AD pathogenesis. However, results from two other phase 3 trials of Aβ immunotherapies, solanezumab and bapineuzumab, do not meet the end points on the cognitive improvement for patients with mild to moderate AD (47, 48), suggesting that the intrinsic characteristics associated with Aβ monoclonal antibodies would dictate their biological efficacy as AD immunotherapy. There is also an urgent need to identify novel pharmacological targets for AD therapies, in

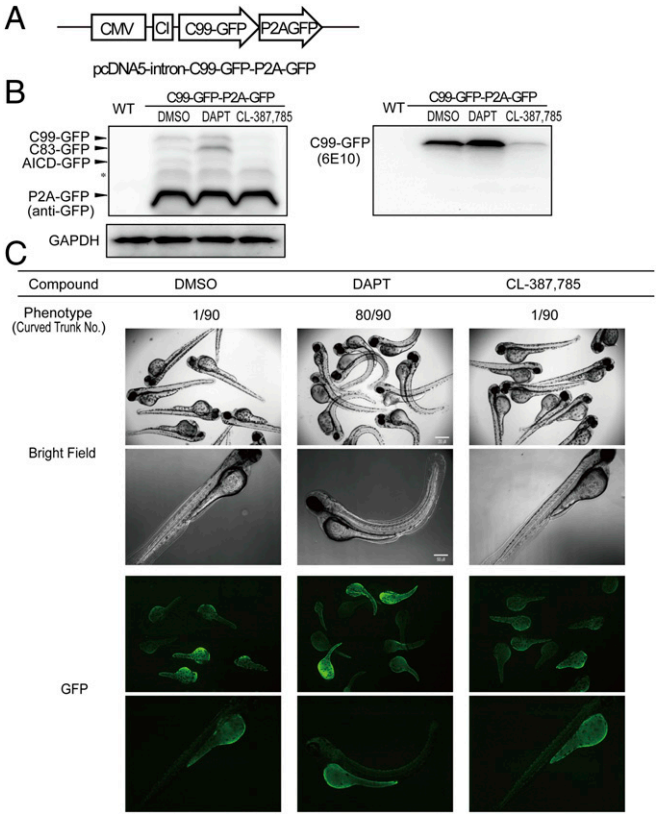

Fig. 7. CL-387,785 can effectively reduce the levels of C99 and AICD without perturbing Notch-dependent somite development in a zebrafish model of amyloidopathy. (*A*) Schematic presentation of the DNA construct encoding recombinant C99-GFP-P2A-GFP. CI, chimeric intron; CMV, human cytomegalovirus promoter; P2A, porcine teschovirus 2A peptide. (*B*) Zebrafish embryos at the one-cell stage were injected with C99-GFP-P2A-GFP plasmid and treated with the indicated compounds from 48 h postfertilization (hpf) to 72 hpf at 28 °C. Clarified lysates derived from treated embryos were analyzed by Western blotting with anti-GFP (for C99, C83, AICD, and P2A-GFP plasmid injection control), anti-Aβ1–16 (6E10, for full-length C99), and anti-GAPDH. The asterisk indicates unidentified bands. WT, wild type. (*C*) Phenotypes of C99-expressing zebrafish embryos treated with the indicated compounds were imaged by bright-field microscopy and fluorescence microscopy. The number of embryos exhibiting a curved trunk at 72 hpf was recorded ($n = 90$).

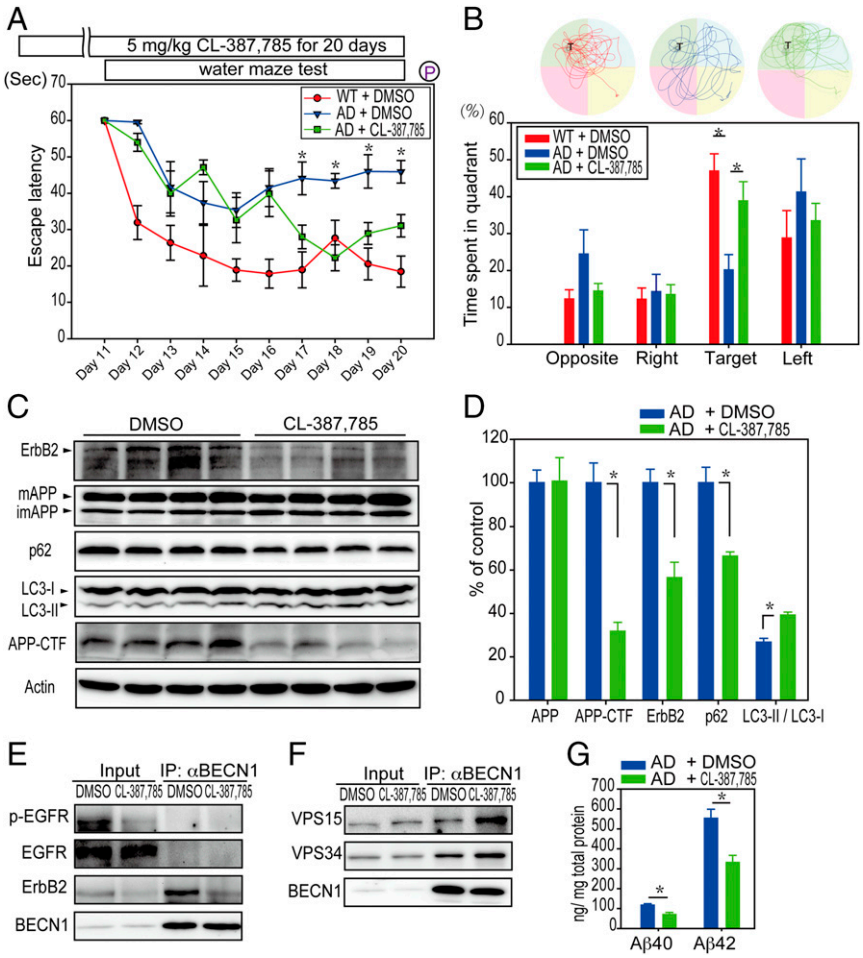

Fig. 8. Inhibition of ErbB2 by CL-387,785 significantly improved learning and memory in APP/PS1 transgenic mice. (*A*) Fifteen-month-old mice were given daily oral doses of vehicle (DMSO) or 5 mg/kg CL-387,785 for 20 d. Escape latencies from days 11–20 are shown as the means ± SEM, and were analyzed by two-way ANOVA (*$P < 0.05$) ($n = 4$). P, probe test. (*B*) Tracking maps and time spent in each of the four quadrants for 90 s on day 21. Data are shown as the means ± SEM, and were analyzed by two-way ANOVA (*$P < 0.05$). T indicates the target quadrant where the invisible platform is located. Western blotting (*C*) and quantitative results (*D*) of the right brains of mice after drug treatment are shown. The quantitative data are shown as the mean ± SEM, and were analyzed by Student's *t* tests. *$P < 0.05$. (*E* and *F*) Homogenized brain lysates from the DMSO or CL-387,785 treatment group were mixed and immunoprecipitated with αBECN1. (*G*) Homogenized brain lysates were dissolved in 5 M guanidine HCl and processed for determination of Aβ40 and Aβ42 using colorimetric Aβ40- and Aβ42-specific ELISA kits. Data were normalized to total protein concentration, and analyzed by Student's *t* tests (mean ± SEM, *$P < 0.05$).

addition to anti-Aβ approaches. We and others have proposed that autophagic clearance of proteinopathy in AD would be an ideal alternative target (14, 33, 34). This notion is substantiated by the autophagy-related pathology found in AD brain evidenced by abnormal acidified lysosomes, accumulated amyloid plaques, and Tau fibrils (49). Furthermore, the down-regulation of PS1 can result in impaired lysosome function, reduced p62 expression, and defective Tau proteostasis (50, 51). On the other hand, dysfunction of autophagy elicited by decreased Beclin-1 expression leads to increased levels of intraneuronal and extracellular Aβ in an AD mouse model (52), whereas induction of autophagy by rapamycin can reduce Aβ42 accumulation, Tau hyperphosphorylation, and oxidative stress to ameliorate cognitive impairment in AD transgenic mice (53). Most intriguingly, a small-molecule enhancer of autophagy (SMER28) is found to suppress the production of Aβ and APP-CTFs effectively, without significant changes in the levels of APLP1 and Notch signaling (54). Our findings that augmentation of autophagic flux by ErbB2 inhibition can preferentially reduce the steady-state levels of C99 and secreted Aβ thus favor a model in which autophagy could be an alternative pharmacological target for the development of novel AD therapies.

Members of the ErbB receptor tyrosine kinase family are highly expressed in the central nervous system of vertebrates, where they are essential for neural development (55–57). ErbBs form various homodimers and heterodimers to activate downstream signaling pathways upon ligand binding (58, 59). A recent study showed that activated ErbB1 can inhibit autophagy by mediating tyrosine phosphorylation of Beclin-1 to modulate Vps34 kinase activity (19). On the contrary, ErbB1 also works as an autophagy initiator by interacting with Rubicon in a kinase-independent manner (60). Our data revealed that either overexpression or knockdown of EGFR/ErbB1 simultaneously increased the levels of C99 and AICD (Fig. 3 *D* and *F*), suggesting that ErbB1 might play dual roles in the regulation of autophagy pending different cellular contexts. In the present study, we provided direct evidence demonstrating that ErbB2 can actively govern the proteostasis of the uncleaved γ-secretase substrate (C99) and the cleaved product (AICD) (Fig. 3 *D*, *F*, and *H*), most likely through modulation of autophagic flux. Our findings suggest that ErbB2 can cause disassembly of the Beclin-1–Vps34–Vps15 complex, and thereby inhibit the initiation of autophagy. Down-regulation of ErbB2 through the use of CL-387,785 or shErbB2 rescues the formation of the Beclin-1–Vps34–Vps15 complex. Reduction of

ErbB2 not only decreases C99 and AICD but also concomitantly attenuates Aβ production without significantly affecting the physiological function of γ-secretase (unchanged Notch signaling). Nonetheless, our findings are in line with the current concept that aberrant autophagic flux is key to the proteinopathy-elicited pathogenesis of neurodegenerative diseases (14, 61). The aberrant expression/activation of ErbB2 may thus predispose toward the development of AD.

The APP-CTFs and AICD also contribute to the pathogenesis of AD in various in vivo models (62, 63). Because Aβ-elicited neurotoxicity can initiate the pathological propagation of AD (3, 64), the detrimental effects elicited by APP-CTFs, including C99, can synergistically exacerbate Aβ-induced neurotoxicity to give rise to the fully developed AD pathology (65). A previous study showed that phosphorylated ErbB1 mediates Aβ42-induced memory loss in AD transgenic mice and that treatments with an ErbB1 kinase inhibitor can rescue memory loss, but not Aβ aggregation (20). However, the ErbB1 kinase inhibitor is only effective in disassociating the phosphorylated ErbB1 from Beclin-1 to prevent ErbB1-mediated phosphorylation of Beclin-1 and reactivate autophagy (19). At a resting state in the absence of EGF signal, ErbB1 does not interact with Beclin-1 and plays no significant role in the regulation of autophagy initiation, which might be the reason why ErbB1 kinase inhibition cannot promote the clearance of Aβ (19, 60) (Figs. 5*A* and 8*E*). On the other hand, the concomitant inhibition of ErbB1 kinase and depletion of ErbB2 by CL-387,785 in our study provide the optimal augmentation of autophagy to trigger simultaneous cognitive improvement and Aβ clearance.

This work presents direct evidence suggesting that ErbB2 in its monomeric form is sufficient to dictate the autophagy-mediated clearance of APP-C99 and that selective down-regulation of ErbB2 can significantly reduce Aβ production without affecting the processing of Notch, a physiological substrate of γ-secretase. Intriguingly, the overexpression of either a KD ErbB2 monomer or constitutively active ErbB2 can induce the dissociation of Beclin-1 from the Vps34–Vps15 autophagy initiation complex, and thus prevent the autophagic clearance of APP-C99, resulting in simultaneous accumulation of APP-C99 and AICD. Consistently, both the chemical inhibition of ErbB2 by CL-387,785 and the RNAi-mediated genetic depletion of ErbB2 can rescue the formation of the Beclin-1–Vps34–Vps15 autophagy initiation complex to propagate the autophagic clearance of APP-C99, leading to a significant reduction in Aβ and a marked improvement in cognitive function (Fig. 8). Our work also demonstrates that the homeostasis of APP processing and Aβ production can be selectively manipulated without compromising the physiological functions of other γ-secretase substrates, such as Notch.

This newly identified function of ErbB2 plays a more prominent role in hindering autophagy initiation than the EGFR/ErbB1 does, because monomeric ErbB2 can effectively disassemble the Beclin-1–Vps34–Vps15 complex. Given that activated EGFR/ErbB1 can bind and phosphorylate Beclin-1 (19), our present study thus suggests a novel molecular basis by which ErbB2 may act as a scaffold of Beclin-1 to keep autophagy activity at a resting state in the absence of EGF signal. These findings thus favor a model in which ErbB2 could work as the gatekeeper of autophagic flux (Fig. S3). In accordance with the increased levels of ErbB2 in the hippocampus of patients with sporadic AD, it is very likely that the ErbB2-mediated suppression of autophagy chronically contributes to the accumulation of APP-CTFs, leading to the uncontrolled increase in Aβ production and the consequent demise of hippocampal neurons during the pathogenesis of sporadic AD. Our data also suggest that ErbB2 might play a more prominent role than EGFR/ErbB1 does in the progression of AD, because EGFR/ErbB1 expression is not significantly changed in AD brain (Fig. 2).

In conclusion, we have identified a critical function of oncogenic receptor tyrosine kinase ErbB2 in its monomeric form and provide proof-of-concept evidence suggesting that increased levels of ErbB2 in the hippocampus could potentially be established as a diagnostic marker of sporadic AD. Our data unveil the molecular basis that positions ErbB2 in the driver's seat to maintain autophagy at a resting state. These findings also favor a model in which ErbB2 serves as the negative regulator of autophagy initiation and implicate ErbB2 as an alternative therapeutic target for novel AD therapies.

Materials and Methods

Study Approval. This study was approved by the Institutional Review Board of the Alzheimer's Disease Center, University of California, Davis. Informed consent to share research tissue after death was obtained from all patients. The procedures for the animal study were approved by the Academia Sinica Institutional Animal Care and Utilization Committee (protocol ID 11-02-131).

Statistics. Quantitative analysis of immunoblots was conducted with Image J (NIH) software (66) by determining the relative intensity of the immunoreactive bands after acquisition of the blot image with the BioSpectrum 600 Imaging System (UVP). The raw immunoblots used for the quantitative and densitometric analyses were included in Dataset S4. Colocalization analysis was performed using Imaris 3D software (Bitplane). Statistical analyses were performed using two-way ANOVA. A value of $P \leq 0.05$ was considered significant.

Online Supplemental Material. Detailed descriptions for additional methods are provided in *SI Materials and Methods*.

ACKNOWLEDGMENTS. We thank Dr. Michael Wolfe for providing human PS1 and NCT cDNA constructs. We thank Dr. Tao-Shih Hsieh for generous support. We thank the Core Facility of the Institute of Cellular and Organismic Biology, Academia Sinica, for technical support. We are also in debt to Dr. Tsu-An Hsu (Institute of Biotechnology and Pharmaceutical Research, National Health Research Institute, Taiwan) for providing kinase inhibitors. The injection of pcDNA5-intron-C99-GFP-P2A-GFP plasmid into zebrafish embryos was performed with assistance from Shih-Hung Lai (National Taiwan University), Yu-Fen Lu (Academia Sinica), Chen-Yu Pan, and Sin-Hong Lai (National Taiwan Ocean University). We also thank Dr. David Root (Broad Institute of MIT and Harvard University) for providing invaluable suggestions and technical assistance related to the RNAi screen. RNAi reagents were obtained from the National RNAi Core Facility located at the Institute of Molecular Biology/Genomic Research Center, Academia Sinica, supported by National Core Facility Program for Biotechnology Grants provided by National Science Council (NSC) Grant 100-2319-B-001-002. We thank the Alzheimer's Disease Center of the University of California, Davis for providing brain samples. This study was supported by Alzheimer's Drug Discovery Foundation/Elan Drug Discovery Award 271214 Elan (to Y.-F.L.); NSC, Taiwan Grant 102-2320-B-001-014 (to Y.-F.L.); Ministry of Science and Technology, Taiwan Grant 103-2320-B-001-016-MY3 (to Y.-F.L.); the Academia Sinica (Y.-F.L.); and U.S. National Institute on Aging Grant P30 AG10129 (to L.-W.J.).

1. Selkoe DJ, Hardy J (2016) The amyloid hypothesis of Alzheimer's disease at 25 years. *EMBO Mol Med* 8:595–608.
2. Wolfe MS, Guénette SY (2007) APP at a glance. *J Cell Sci* 120:3157–3161.
3. Karran E, Mercken M, De Strooper B (2011) The amyloid cascade hypothesis for Alzheimer's disease: An appraisal for the development of therapeutics. *Nat Rev Drug Discov* 10:698–712.
4. Citron M (2010) Alzheimer's disease: Strategies for disease modification. *Nat Rev Drug Discov* 9:387–398.
5. Vassar R, Kovacs DM, Yan R, Wong PC (2009) The beta-secretase enzyme BACE in health and Alzheimer's disease: Regulation, cell biology, function, and therapeutic potential. *J Neurosci* 29:12787–12794.
6. Parks AL, Curtis D (2007) Presenilin diversifies its portfolio. *Trends Genet* 23:140–150.
7. Chaudhury AR, et al. (2003) Neuregulin-1 and erbB4 immunoreactivity is associated with neuritic plaques in Alzheimer disease brain and in a transgenic model of Alzheimer disease. *J Neuropathol Exp Neurol* 62:42–54.
8. Ray S, et al. (2007) Classification and prediction of clinical Alzheimer's diagnosis based on plasma signaling proteins. *Nat Med* 13:1359–1362.
9. Gómez Ravetti M, Moscato P (2008) Identification of a 5-protein biomarker molecular signature for predicting Alzheimer's disease. *PLoS One* 3:e3111.
10. Birecree E, Whetsell WO, Jr, Stoscheck C, King LE, Jr, Nanney LB (1988) Immunoreactive epidermal growth factor receptors in neuritic plaques from patients with Alzheimer's disease. *J Neuropathol Exp Neurol* 47:549–560.
11. Amigoni L, Ceriani M, Belotti F, Minopoli G, Martegani E (2011) Activation of amyloid precursor protein processing by growth factors is dependent on Ras GTPase activity. *Neurochem Res* 36:392–398.
12. Russo C, et al. (2002) Signal transduction through tyrosine-phosphorylated C-terminal fragments of amyloid precursor protein via an enhanced interaction with Shc/Grb2 adaptor proteins in reactive astrocytes of Alzheimer's disease brain. *J Biol Chem* 277:35282–35288.

13. Klionsky DJ, et al. (2016) Guidelines for the use and interpretation of assays for monitoring autophagy (3rd edition). *Autophagy* 12:1–222.
14. Tung YT, et al. (2012) Autophagy: A double-edged sword in Alzheimer's disease. *J Biosci* 37:157–165.
15. Yamamoto A, Cremona ML, Rothman JE (2006) Autophagy-mediated clearance of huntingtin aggregates triggered by the insulin-signaling pathway. *J Cell Biol* 172: 719–731.
16. Tanik SA, Schultheiss CE, Volpicelli-Daley LA, Brunden KR, Lee VM (2013) Lewy body-like α-synuclein aggregates resist degradation and impair macroautophagy. *J Biol Chem* 288:15194–15210.
17. Xilouri M, et al. (2013) Boosting chaperone-mediated autophagy in vivo mitigates α-synuclein-induced neurodegeneration. *Brain* 136:2130–2146.
18. Schaeffer V, et al. (2012) Stimulation of autophagy reduces neurodegeneration in a mouse model of human tauopathy. *Brain* 135:2169–2177.
19. Wei Y, et al. (2013) EGFR-mediated Beclin 1 phosphorylation in autophagy suppression, tumor progression, and tumor chemoresistance. *Cell* 154:1269–1284.
20. Wang L, et al. (2012) Epidermal growth factor receptor is a preferred target for treating amyloid-β-induced memory loss. *Proc Natl Acad Sci USA* 109:16743–16748.
21. Kukar TL, et al. (2008) Substrate-targeting gamma-secretase modulators. *Nature* 453: 925–929.
22. Kounnas MZ, et al. (2010) Modulation of gamma-secretase reduces beta-amyloid deposition in a transgenic mouse model of Alzheimer's disease. *Neuron* 67:769–780.
23. Thathiah A, et al. (2009) The orphan G protein-coupled receptor 3 modulates amyloid-beta peptide generation in neurons. *Science* 323:946–951.
24. Flajolet M, et al. (2007) Regulation of Alzheimer's disease amyloid-beta formation by casein kinase I. *Proc Natl Acad Sci USA* 104:4159–4164.
25. Eisele YS, et al. (2007) Gleevec increases levels of the amyloid precursor protein intracellular domain and of the amyloid-beta degrading enzyme neprilysin. *Mol Biol Cell* 18:3591–3600.
26. He G, et al. (2010) Gamma-secretase activating protein is a therapeutic target for Alzheimer's disease. *Nature* 467:95–98.
27. Liao YF, Wang BJ, Cheng HT, Kuo LH, Wolfe MS (2004) Tumor necrosis factor-alpha, interleukin-1beta, and interferon-gamma stimulate gamma-secretase-mediated cleavage of amyloid precursor protein through a JNK-dependent MAPK pathway. *J Biol Chem* 279:49523–49532.
28. Tung YT, et al. (2008) Sodium selenite inhibits gamma-secretase activity through activation of ERK. *Neurosci Lett* 440:38–43.
29. Szklarczyk D, et al. (2015) STRING v10: Protein-protein interaction networks, integrated over the tree of life. *Nucleic Acids Res* 43:D447–D452.
30. Uhlén M, et al. (2015) Proteomics. Tissue-based map of the human proteome. *Science* 347:1260419.
31. Uhlen M, et al. (2010) Towards a knowledge-based Human Protein Atlas. *Nat Biotechnol* 28:1248–1250.
32. Kenific CM, Debnath J (2015) Cellular and metabolic functions for autophagy in cancer cells. *Trends Cell Biol* 25:37–45.
33. Menzies FM, Fleming A, Rubinsztein DC (2015) Compromised autophagy and neurodegenerative diseases. *Nat Rev Neurosci* 16:345–357.
34. Nixon RA (2013) The role of autophagy in neurodegenerative disease. *Nat Med* 19: 983–997.
35. Kang R, Zeh HJ, Lotze MT, Tang D (2011) The Beclin 1 network regulates autophagy and apoptosis. *Cell Death Differ* 18:571–580.
36. Molejon MI, Ropolo A, Re AL, Boggio V, Vaccaro MI (2013) The VMP1-Beclin 1 interaction regulates autophagy induction. *Sci Rep* 3:1055.
37. Han J, et al. (2013) Interaction between Her2 and Beclin-1 proteins underlies a new mechanism of reciprocal regulation. *J Biol Chem* 288:20315–20325.
38. Sigurdsson HH, Olesen CW, Dybboe R, Lauritzen G, Pedersen SF (2014) Constitutively active ErbB2 regulates cisplatin-induced cell death in breast cancer cells via pro- and anti-apoptotic mechanisms. *Mol Cancer Res* 13:63–77.
39. Ward TM, et al. (2013) Truncated p110 ERBB2 induces mammary epithelial cell migration, invasion and orthotopic xenograft formation, and is associated with loss of phosphorylated STAT5. *Oncogene* 32:2463–2474.
40. Yang L, Li Y, Zhang Y (2014) Identification of prolidase as a high affinity ligand of the ErbB2 receptor and its regulation of ErbB2 signaling and cell growth. *Cell Death Dis* 5: e1211.
41. Penuel E, Akita RW, Sliwkowski MX (2002) Identification of a region within the ErbB2/HER2 intracellular domain that is necessary for ligand-independent association. *J Biol Chem* 277:28468–28473.
42. Xia W (2010) Exploring Alzheimer's disease in zebrafish. *J Alzheimers Dis* 20:981–990.
43. Arslanova D, et al. (2010) Phenotypic analysis of images of zebrafish treated with Alzheimer's gamma-secretase inhibitors. *BMC Biotechnol* 10:24.
44. Hardy J, Allsop D (1991) Amyloid deposition as the central event in the aetiology of Alzheimer's disease. *Trends Pharmacol Sci* 12:383–388.
45. Rafii MS, Aisen PS (2015) Advances in Alzheimer's disease drug development. *BMC Med* 13:62.
46. Sevigny J, et al. (2016) The antibody aducanumab reduces Aβ plaques in Alzheimer's disease. *Nature* 537:50–56.
47. Doody RS, et al.; Alzheimer's Disease Cooperative Study Steering Committee; Solanezumab Study Group (2014) Phase 3 trials of solanezumab for mild-to-moderate Alzheimer's disease. *N Engl J Med* 370:311–321.
48. Salloway S, et al.; Bapineuzumab 301 and 302 Clinical Trial Investigators (2014) Two phase 3 trials of bapineuzumab in mild-to-moderate Alzheimer's disease. *N Engl J Med* 370:322–333.
49. Peric A, Annaert W (2015) Early etiology of Alzheimer's disease: Tipping the balance toward autophagy or endosomal dysfunction? *Acta Neuropathol* 129:363–381.
50. Lee JH, et al. (2010) Lysosomal proteolysis and autophagy require presenilin 1 and are disrupted by Alzheimer-related PS1 mutations. *Cell* 141:1146–1158.
51. Tung YT, et al. (2014) Presenilin-1 regulates the expression of p62 to govern p62-dependent tau degradation. *Mol Neurobiol* 49:10–27.
52. Pickford F, et al. (2008) The autophagy-related protein beclin 1 shows reduced expression in early Alzheimer disease and regulates amyloid beta accumulation in mice. *J Clin Invest* 118:2190–2199.
53. Cai Z, Yan LJ (2013) Rapamycin, autophagy, and Alzheimer's disease. *J Biochem Pharmacol Res* 1:84–90.
54. Tian Y, Bustos V, Flajolet M, Greengard P (2011) A small-molecule enhancer of autophagy decreases levels of Abeta and APP-CTF via Atg5-dependent autophagy pathway. *FASEB J* 25:1934–1942.
55. Fox IJ, Kornblum HI (2005) Developmental profile of ErbB receptors in murine central nervous system: Implications for functional interactions. *J Neurosci Res* 79:584–597.
56. Sharif A, et al. (2009) Differential erbB signaling in astrocytes from the cerebral cortex and the hypothalamus of the human brain. *Glia* 57:362–379.
57. Lyons DA, et al. (2005) erbb3 and erbb2 are essential for schwann cell migration and myelination in zebrafish. *Curr Biol* 15:513–524.
58. Endres NF, Engel K, Das R, Kovacs E, Kuriyan J (2011) Regulation of the catalytic activity of the EGF receptor. *Curr Opin Struct Biol* 21:777–784.
59. Citri A, Yarden Y (2006) EGF-ERBB signalling: Towards the systems level. *Nat Rev Mol Cell Biol* 7:505–516.
60. Tan X, Thapa N, Sun Y, Anderson RA (2015) A kinase-independent role for EGF receptor in autophagy initiation. *Cell* 160:145–160.
61. Wong YC, Holzbaur EL (2015) Autophagosome dynamics in neurodegeneration at a glance. *J Cell Sci* 128:1259–1267.
62. Ghosal K, et al. (2009) Alzheimer's disease-like pathological features in transgenic mice expressing the APP intracellular domain. *Proc Natl Acad Sci USA* 106: 18367–18372.
63. Jeong YH, et al. (2006) Chronic stress accelerates learning and memory impairments and increases amyloid deposition in APPV717I-CT100 transgenic mice, an Alzheimer's disease model. *FASEB J* 20:729–731.
64. Canevari L, Abramov AY, Duchen MR (2004) Toxicity of amyloid beta peptide: Tales of calcium, mitochondria, and oxidative stress. *Neurochem Res* 29:637–650.
65. Kim SH, Suh YH (1996) Neurotoxicity of a carboxyl-terminal fragment of the Alzheimer's amyloid precursor protein. *J Neurochem* 67:1172–1182.
66. Schindelin J, Rueden CT, Hiner MC, Eliceiri KW (2015) The ImageJ ecosystem: An open platform for biomedical image analysis. *Mol Reprod Dev* 82:518–529.
67. Schroeter EH, Kisslinger JA, Kopan R (1998) Notch-1 signalling requires ligand-induced proteolytic release of intracellular domain. *Nature* 393:382–386.
68. Kimberly WT, et al. (2003) Gamma-secretase is a membrane protein complex comprised of presenilin, nicastrin, Aph-1, and Pen-2. *Proc Natl Acad Sci USA* 100: 6382–6387.
69. Karolewski BA, Watson DJ, Parente MK, Wolfe JH (2003) Comparison of transfection conditions for a lentivirus vector produced in large volumes. *Hum Gene Ther* 14: 1287–1296.
70. Angers S, et al. (2000) Detection of beta 2-adrenergic receptor dimerization in living cells using bioluminescence resonance energy transfer (BRET). *Proc Natl Acad Sci USA* 97:3684–3689.
71. Boute N, Jockers R, Issad T (2002) The use of resonance energy transfer in high-throughput screening: BRET versus FRET. *Trends Pharmacol Sci* 23:351–354.
72. Kim JH, et al. (2011) High cleavage efficiency of a 2A peptide derived from porcine teschovirus-1 in human cell lines, zebrafish and mice. *PLoS One* 6:e18556.
73. Vorhees CV, Williams MT (2006) Morris water maze: Procedures for assessing spatial and related forms of learning and memory. *Nat Protoc* 1:848–858.